Giant Charge-to-Spin Conversion Efficiency in SrTiO₃-Based Electron Gas Interface

Huaiwen Yang,[1] Boyu Zhang,[1] Xueying Zhang,[1,2] Xi Yan,[3] Wenlong Cai,[1] Yinglin Zhao,[2] Jirong Sun,[3] Kang L. Wang,[4] Dapeng Zhu,[1,2,*] and Weisheng Zhao◉[1,†]

[1] *Fert Beijing Institute, BDBC, School of Microelectronics, Beihang University, Beijing 100191, China*

[2] *Beihang-Goertek Joint Microelectronics Institute, Qingdao Research Institute, Beihang University, Qingdao 266000, China*

[3] *Beijing National Laboratory for Condensed Matter Physics and Institute of Physics, Chinese Academy of Sciences, Beijing 100190, China*

[4] *Department of Electrical Engineering, University of California, Los Angeles, California 90095, USA*

Spin current induced by a charge current has been extensively explored to electrically manipulate magnetism and high charge-to-spin conversion efficiency is expected to enable a low power spin-orbit torque (SOT) switching mechanism. We report on experimental results that demonstrate a charge current flowing in-plane in an oxide Rashba-Edelstein two-dimensional electron gases (2DEGs) interface that can efficiently generate a spin current, and a strong SOT in an adjacent permalloy layer is observed by spin-torque ferromagnetic resonance. The charge-to-spin conversion efficiency $|\theta_{CS}|$ is up to a value of 0.9 for a simple Ar⁺-etched SrTiO₃/NiFe structure, which is much larger than that of heavy meals, and the structure can be easily fabricated by magnetron sputtering. In addition, the spin-orbital coupling in the SrTiO₃/LaAlO₃ interface is more efficient and $|\theta_{CS}|$ can be increased up to 1.8 for the SrTiO₃/LaAlO₃/NiFe device, whereas it is only 0.6 for a SrTiO₃/LaTiO₃/NiFe device. These results will enable the realization of SOT devices based on SrTiO₃-based 2DEGs for low power nonvolatile memory and logic.

I. INTRODUCTION

Two-dimensional electron gases (2DEGs) at the interface of oxides were first discovered at SrTiO₃/LaAlO₃ (STO/LAO) interfaces, which attracted significant attention because of their unique physical properties and prospective applications [1]. A number of exotic properties including ultrahigh mobility [2], local magnetism [3], and superconductivity [4,5] have been observed in these systems. The microscopic mechanism of conductivity is still in debate, and three competing theories have been proposed to explain the formation of 2DEGs [6–8]. With the emergence of different 2DEGs, alternative approaches have been explored to investigate the effective tuning of their carrier mobility and interfacial magnetism [9–12].

According to the literature, spin-orbital coupling is very strong in 2DEGs [11,12]. Recently, mutual spin-charge conversion at heterointerfaces based on the Edelstein effect (EE) and inverse Edelstein effect (IEE) has emerged as a topic of interest in 2DEGs. Edelstein declared in 1990 that a spin-current can be induced by a charge current flowing in inversion antisymmetric 2DEGs [13], as described by the following relation

$$J_S \propto \alpha_R(\hbar/e)(\vec{z} \times \overrightarrow{J_C}), \tag{1}$$

where α_R is the Rashba parameter, $\vec{z}$ is the interfacial electric field direction perpendicular to the 2DEGs, and $\overrightarrow{J_C}$ is the charge current. The IEE is the opposite effect of the EE, which means that spin accumulation in inversion asymmetric 2DEGs can generate an in-plane electric field perpendicular to the direction of the spin polarization. IEE has been observed at room temperature in STO/LAO 2DEGs by Song *et al.* [14]. This effect was also observed by Lesne *et al.* [15] at 7 K, and the authors proved that the efficiency for spin-to-charge conversion is very high. It was further determined that the spin transport in STO/LAO is via the d electrons and the diffusion length is up to 300 nm. These are very promising properties with respect to the design of alternative spintronic devices [16]. Recently, a charge-to-spin conversion was reported at room temperature for the STO/LAO system [17]. These results hint at the great potential of the oxide 2DEGs for applications to spintronics, which have attracted extensive attention.

*zhudp@buaa.edu.cn
†weisheng.zhao@buaa.edu.cn

034004-1

Spin-orbit torque (SOT) is a very promising way to manipulate magnetism using a pure charge current. A charge current can generate a spin current in the out-of-plane direction when it flows through a layer with a strong spin-orbital coupling. The induced spin current can generate a SOT in an adjacent ferromagnetic (FM) layer, causing a change in the direction of the magnetization. In fact, SOT switching has been successfully applied to switch the direction of the magnetization for magnetic tunneling junctions (MTJs) [18], topological insulators [19], and antiferromagnets [20]. For example, Han *et al.* [19] realized room-temperature magnetic switching for MTJs using a topological insulator. In addition, many systems with spin-orbital coupling have been explored for the purpose of manipulating the direction of magnetization using an electric current.

In this report, we present results on the generation of a spin-current from a charge current via the EE and the SOT generated by Rashba-Edelstein spin-splitting oxide 2DEGs residing in STO, based on the technique of spin-torque ferromagnetic magnetic resonance (ST-FMR). The charge-to-spin conversion efficiency $|\theta_{CS}|$ is up to 0.9 for an Ar^+-etched $SrTiO_3/NiFe$ ($Ar^+STO/NiFe$) device, 1.8 for $SrTiO_3/LaAlO_3/NiFe$ (STO/LAO/NiFe), and 0.6 for $SrTiO_3/LaTiO_3/NiFe$ (STO/LTO/NiFe) at room temperature for measurement at the frequency of 6 GHz. These values are much larger than that of 0.07 in Pt [21]. Furthermore, the Gilbert damping coefficient and the effective magnetic field are investigated. In this report, an efficient and promising way to manipulate magnetization using a pure current is proposed.

II. EXPERIMENTAL DETAILS AND RESULTS

A. Sample fabrication

(1) An Ar^+-etched STO: $SrTiO_3$ (100) substrate ($5 \times 5 \times 0.5$ mm^3) is precleaned by Ar^+ ions for 120 s by magnetron sputtering, which is to make the surface conductive. (2) STO/LAO and STO/LTO: 10 unit cells of $LaAlO_3$ and $LaTiO_3$ films are prepared on TiO_2-terminated STO (100) substrates ($5 \times 5 \times 0.5$ mm^3) using a pulsed laser (248 nm) ablation technique at a temperature of 800°C and an oxygen pressure of 10^{-4} mbar. The fluence of the laser pulses is 1.5 J/cm^2 and the repetition rate is 1 Hz. Both samples are transferred into a high vacuum chamber (base pressure less than 2×10^{-8} Torr) for magnetron sputtering to grow NiFe (5 nm)/SiO$_2$ (5 nm) layers at room temperature. The sputtering pressure is 3 mTorr. The multilayer films are patterned into standard Hall bars (120×10 μm^2) and rectangular-shaped strips (20×20 μm^2) for anisotropy magnetoresistance (AMR) and ST-FMR measurements, respectively, using optical lithography and dry etching. Cr (10 nm)/Au (100 nm) metal stacks are deposited as contacts for electrical measurements.

B. ST-FMR measurements

A microwave-frequency (GHz) charge current I_{rf} with a power of 15 dBm from the signal generator is applied to the device, and the dc voltage is simultaneously measured using a bias tee. An in-plane magnetic field with a fixed angle θ_H of 45° with respect to the current axis is swept from 0.2 T to −0.2 T. All the ST-FMR experiments are performed at room temperature. The resistance, Hall resistance, and AMR are measured using a physical properties measurement system (PPMS). The temperature-dependent transport properties are measured using the van der Pauw method.

A schematic diagram of the ST-FMR measurement setup and sample structure is shown in Fig. 1(a). When the ac current flows through the 2DEGs and NiFe, the accumulation of spins takes place simultaneously in the 2DEGs due to EE. These accumulated spins generate a spin current J_S in the orthogonal direction, and thus exert a spin torque on the NiFe layer. The oscillating current-induced torque causes the NiFe magnetization process, thus yielding resistance oscillations due to the AMR of the bilayer films. The resonance line shape can be measured using a direct voltage V_{mix}. Figure 1(b) represents the expected qualitative Fermi contours of the Rashba-Edelstein 2DEGs. At the Fermi level (E_F), the spin textures of the outer and inner circles are opposite to each other. Whether the spin texture is clockwise or counterclockwise depends on the sign of α_R and the definition of the normal direction. The room temperature Hall measurement is shown in Fig. 1(c). The Hall voltage is linear with the magnetic field, which indicates that only the normal Hall effect exists. Based on these data, we obtain a sheet carrier density of 2.7×10^{13} cm^{-2} and a carrier mobility of 7.78 cm^2/(V s) at room temperature. The details of temperature-dependent Hall resistance, the calculated carrier density, and carrier mobility are presented in the Supplemental Material [22]. From the angle-dependent magnetoresistance measurements, the in-plane anisotropy magnetoresistance is determined to be approximately 0.8% as shown in Fig. 1(d). The spin Hall magnetoresistance is approximately 0.25%.

C. ST-FMR results

A typical ST-FMR spectrum measured for the $Ar^+STO/NiFe$ device is shown in Fig. 1(e). The symmetric component is much larger than the antisymmetric component in the system. While the antisymmetric component V_{anti} arises from the Oersted field torque induced by the charge current flowing in the 2DEGs layer, the symmetric voltage V_{sym} is attributed to the spin torque $\tau_{\parallel}$, which corresponds to the spin-current density J_S. By quantitative evaluation of V_{sym} and V_{anti}, the interface charge-to-spin conversion efficiency $|\theta_{CS}|$ can be deduced.

Figure 2(a) shows the ST-FMR spectra for the sample with a 5-nm-thick NiFe layer on Ar^+-etched STO in the
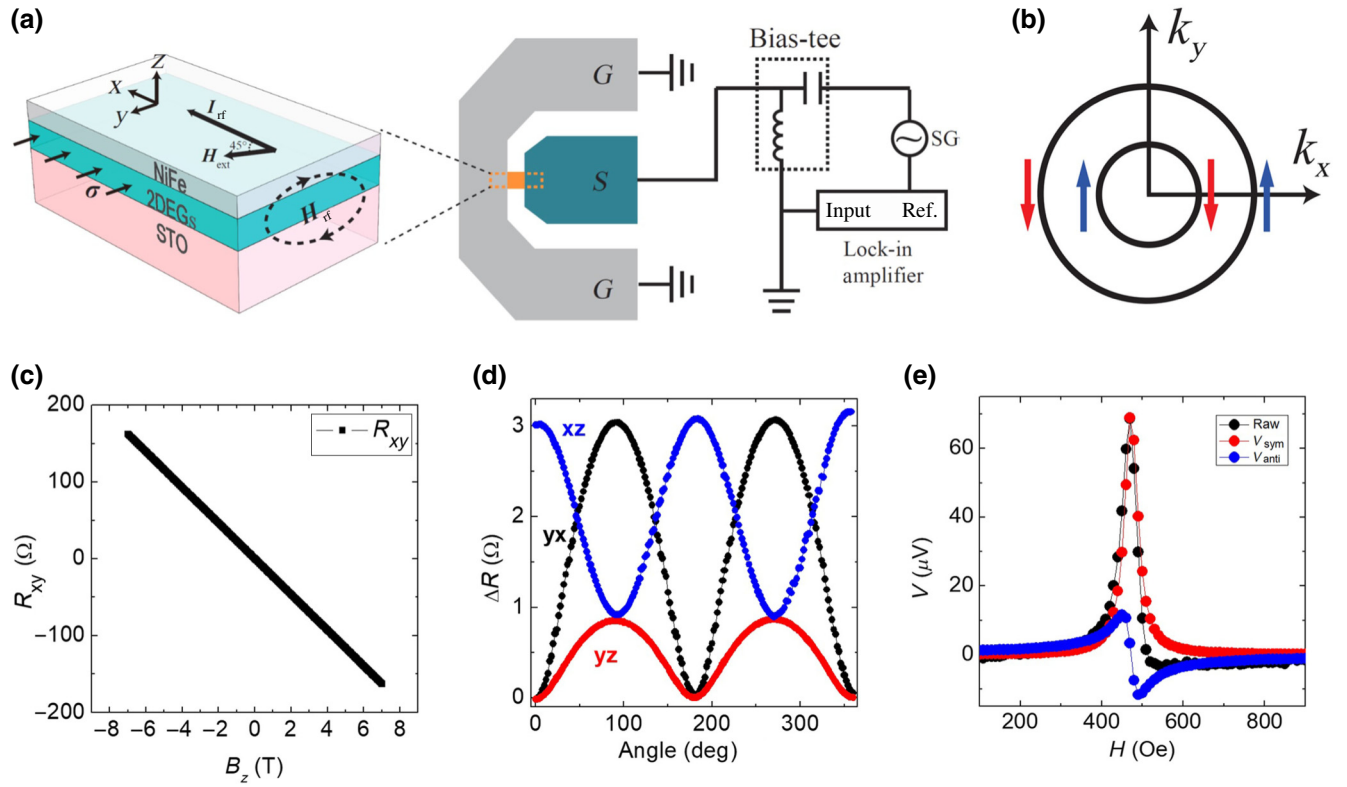
FIG. 1. (a) The schematic diagram of ST-FMR and the film layer structures [17]. (b) The Fermi contours of Rashba-Edelstein 2DEGs. (c) The Hall resistance measurement of Ar^+-etched STO surface at room temperature. (d) Angle-dependent magnetoresistance measurements of Ar^+STO/NiFe device at 2.5 T and 300 K for three different rotation planes. (e) ST-FMR signals of the Ar^+STO/NiFe device obtained at 6 GHz, 15 dBm, and 300 K (black dot). Red: the symmetric Lorentzian component. Blue: the antisymmetric Lorentzian component. Solid lines are the results of curve fitting.

frequency range of 5 to 9 GHz. The amplitude decreases as the frequency increases. From the inset figure, it is evident that V_{mix} is opposite when the magnetic field is reversed. The measured curve can be well fitted by a Lorentzian function consisting of a symmetric and an antisymmetric Lorentzian component as follows [21,23]:

$$V_{mix} = S\frac{\Delta^2}{\Delta^2 + (H_{ext} + H_0)^2} + A\frac{\Delta(H_{ext} + H_0)}{\Delta^2 + (H_{ext} + H_0)^2},$$
(2)

where Δ is the line width (full width at half maximum), H_0 is the resonant magnetic field, S is the symmetric Lorentzian coefficient, and A is the antisymmetric Lorentzian coefficient. By fitting the curve, the parameters of Δ, S, A, and H_0 can be obtained.

Figure 2(b) is the ST-FMR signal of the three devices in 6 GHz. The signal amplitude of Ar^+STO/NiFe is much larger than that of the other two devices, which should be due to the fact that no insulator exists between the 2DEGs and FM layer in Ar^+STO/NiFe. From the resonant peak position, we can see the resonant field of STO/LTO/NiFe is about 480 Oe, which is larger than that of the other two

devices. Figure 2(c) shows the resonant frequency f as a function of the resonant field H_0. For the three samples, the resonant field changes slightly. As the resonant frequency increases, the resonant field also increases in all the samples. The curve can be fitted using the Kittel equation shown below [21,24,25]

$$f = (\gamma/2\pi)[\mu_0 H_0(\mu_0 H_0 + 4\pi M_{eff})]^{1/2},$$
(3)

where γ is the gyromagnetic ratio. The $4\pi M_{eff}$ represents the contribution of interfacial anisotropy. This value is calculated to be 0.93 T for Ar^+STO/NiFe, 0.92 T for the STO/LAO/NiFe, and 0.90 T for STO/LTO/NiFe, which are all larger than the 0.85 T for Pt/NiFe structures [26]. These results indicate that the interfacial anisotropy is very large in the three devices.

Magnetic damping is studied based on the frequency dependence of the resonance line width Δ as shown in Fig. 2(d). Δ increases as the frequency increases for all three samples, but Δ increases slower in STO/LTO/NiFe devices. This parameter usually includes intrinsic and extrinsic origins, which is given by [24,25]

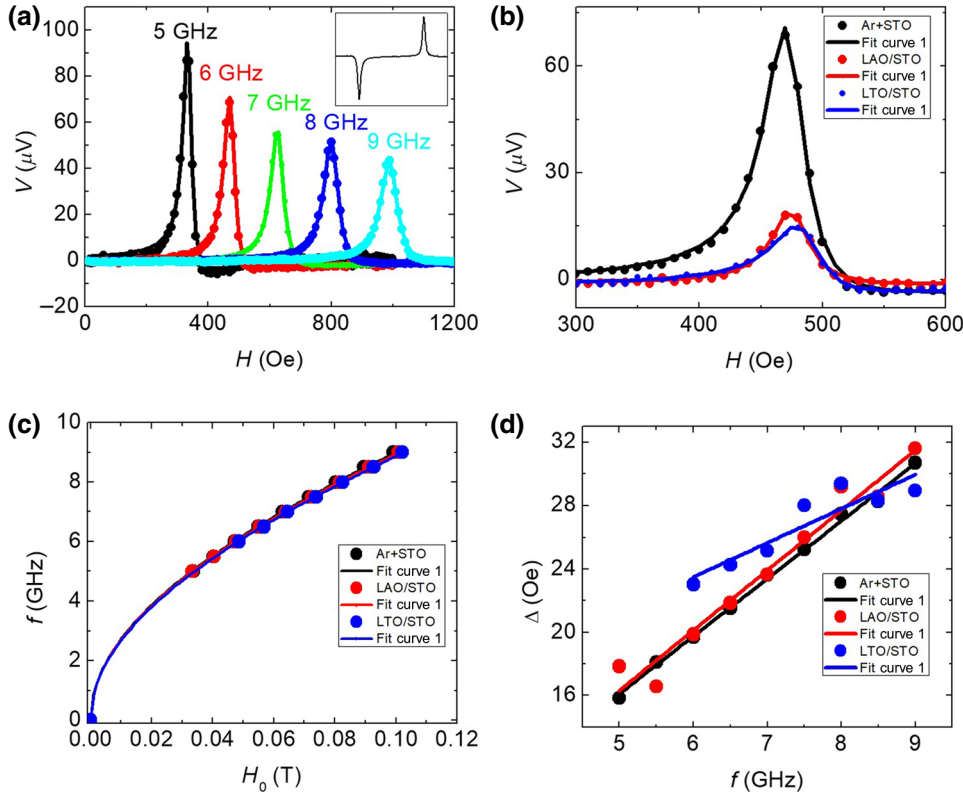$$\Delta = \Delta_0 + (2\pi\alpha/\gamma)f,$$
(4)

FIG. 2.   (a) The ST-FMR signal of the $Ar^+STO/NiFe$ device in the frequency range of 5 to 9 GHz (dot) and fitting curve (line) at room temperature. The inset is the full magnetic field range of the ST-FMR signal at 6 GHz. (b) The ST-FMR signals of the $Ar^+STO/NiFe$, STO/LAO/NiFe, and STO/LTO/NiFe devices in 6 GHz (c) Resonant frequency f as a function of the resonant field H_0. The solid curve represents a fit to the Kittel formula. (d) The line width Δ extracted from the fitting of the ST-FMR signal versus the resonant frequency f. The solid lines are the linear fittings.

where Δ_0 is the extrinsic contribution (e.g., inhomogeneous broadening) to the line width, which is usually independent of frequency. The second term is the intrinsic contribution, which is linearly proportional to the frequency and related to the Gilbert damping coefficient α. The Gilbert damping coefficient is approximately 0.01 for $Ar^+STO/NiFe$ and 0.011 for the STO/LAO/NiFe device, which matches well with the result of the NiFe film from spin valves [27], whereas it is only 0.006 for the STO/LTO/NiFe device.

Using this result, the ratio of the spin-current density entering the NiFe to the charge-current density in the 2DEGs can then be determined quantitatively in a simple way based on the ratio of the symmetric and antisymmetric components of the resonance curve as follows [21]:

$$|\theta_{CS}| = \frac{J_S}{J_C} = \left|\frac{S}{A}\right| \frac{e\mu_0 M_S t d}{\hbar}[1 + (4\pi M_{eff}/H_{ext})]^{1/2} \quad (5)$$

where J_S is the spin-current density (A m^{-2}), J_C is the charge-current density (A m^{-2}) in the entire 2DEGs layer, M_S is the saturation magnetization of NiFe, t is the thickness of the NiFe layer, and d is the thickness of the 2DEGs conducting layer.

From Fig. 3(a), we can determine that the symmetric component of $Ar^+STO/NiFe$ is approximately 70 μV at 6 GHz, which is induced by the spin-orbit torque in the film. As the frequency increases, this value decreases.

The antisymmetric component shows the same trend. In calculating the charge-to-spin conversion efficiency $|\theta_{CS}|$, the conductive thickness of the 2DEGs is chosen as 10 nm according to the published report [28]. As shown in Fig. 3(b), the calculated $|\theta_{CS}|$ is approximately 0.9 at 6 GHz for the $Ar^+STO/NiFe$ device, which is the same order as in the topological insulator case [29]. In the STO/LAO/NiFe device, the symmetric component is only 20 μV at 6 GHz, and the antisymmetric component is also very small. According to Eq. (5), the charge-to-spin efficiency $|\theta_{CS}|$ of the STO/LAO/NiFe device is calculated to be approximately 1.8, which is larger than that of the Ar^+-etched STO and STO/LTO devices. Here, it is surprising that a high SOT efficiency (0.6–1.8) presents in all the three $SrTiO_3$-based 2DEGs systems, as compared with the values of 0.06–0.3 for normal heavy metals (HM) such as Pt, Ta, and W [18,21,24]. It is worth mentioning that strong spin-orbit coupling and giant spin splitting have been experimentally observed for Ar^+-etched $SrTiO_3$, $LaAlO_3/SrTiO_3$, and $LaTiO_3/SrTiO_3$ 2DEGs systems, with the Rashba parameter α_R in range of approximately 0.01–0.2 eV Å, which is two to three orders of magnitude larger than the common semiconductors (e.g., approximately 3×10^{-4} eV Å for GaAs) [30]. Although the origin of the giant spin splitting in the $SrTiO_3$-based systems is still a subject of debate, we believe the efficient SOT in these $SrTiO_3$-based systems is closely related to the giant spin splitting in the electronic structure of 2DEGs.
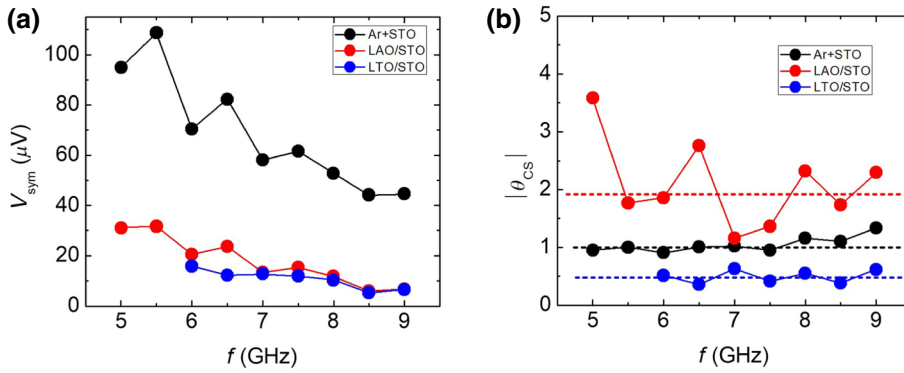
FIG. 3. (a) The symmetric component extracted from the fitting of the ST-FMR signal versus the resonant frequency f for the three devices. (b) Charge-to-spin conversion efficiency $|\theta_{CS}|$ determined from Eq. (5) at different frequencies.

The interfacial SOT efficiency λ (nm^{-1}) can be calculated as $\lambda = (J_s)/(J_c t_{2DEGs})$. The value is approximately 0.09 nm^{-1} for Ar$^+$STO/NiFe, 0.18 nm^{-1} for STO/LAO/NiFe, and 0.06 nm^{-1} for STO/LTO/NiFe, where the STO/LAO/NiFe device shows the largest λ. From the conduction mechanism of the three 2DEGs, this difference is analyzed. The Ar$^+$-etched STO surface mixes the Ti$^+$ with Ti$^+$ as a result of the oxygen vacancy induced by etching. In the STO/LAO interface, the conductivity arises from the charge transfer from the LaAlO$_3$ bulk to the interface. For these two samples, the induced interface electric field is different, thus the spin-orbital coupling is different. In STO/LTO/NiFe, less charge transfer exists and the oxygen vacancy is also less than that of other devices, so its SOT efficiency is the smallest among the three devices. From the charge-to-spin efficiency, it can be conjectured that the spin-orbital coupling of the STO/LAO interface is probably the largest.

III. DISCUSSION

As is known, in a HM/FM structure, after the spin current generation in the HM layer, the spins need to cross the HM/FM interface and then exert spin torques on the FM layer. Recent works have demonstrated the important role of the spin transmission process in the resultant SOT efficiency in HM/FM bilayers [31–33]. Here, for the SrTiO$_3$-based 2DEGs systems, in addition to the differences in the 2DEGs conducting mechanism and probably

the spin-orbital coupling strength, the spin transmission process from the 2DEGs to the ferromagnetic NiFe layer is also different. While the 2DEGs is directly in contact with the NiFe in the Ar$^+$STO/NiFe device where the spin transmission process is similar to that in HM/FM structures [31], the spins need to pass through an insulating LAO (LTO) layer of approximately 4 nm to exert the spin torques on the NiFe layer in the STO/LAO/NiFe (STO/LTO/NiFe) device. Considering that the insulating layer thickness is much larger than the usual overlap distance (<2 nm) of the electron wave functions on either side of an insulating layer [34,35], a possible spin transmission mechanism in the STO/LAO/NiFe (STO/LTO/NiFe) device might be the inelastic tunneling mechanism via localized states in the LAO (LTO) band gap, as recently demonstrated by Wang *et al.* [17].

Figure 4(a) shows microwave-power-dependent ST-FMR signal in the Ar$^+$STO/NiFe device at 6 GHz from 2 to 15 dBm. As the power increases, the ST-FMR signal also increases. The voltage of the symmetric component V_{sym} in the three devices varies linearly with the power, as in Fig. 4(b), which demonstrates the magnetization precession is in the linear regime.

It is worth noting that previous investigations have revealed a large variation of the conducting thickness in the SrTiO$_3$-based 2DEG systems, and the estimation of the SOT efficiency strongly depends on these conducting thickness values. For instance, conducting layer ranges from 5 to 60 nm have been reported in the Ar$^+$-etched
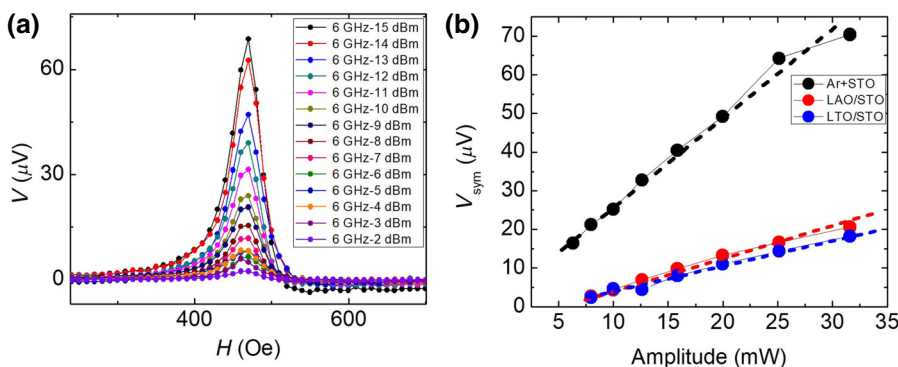

FIG. 4. (a) Microwave power dependence of the ST-FMR signal in the Ar$^+$STO/NiFe device. (b) The microwave power dependence of V_{sym} extracted from the ST-FMR signals in the three devices.

SrTiO$_3$ 2DEGs [36–38], which would lead to a SOT efficiency of 0.45–5.4 for the Ar$^+$STO/NiFe device. Thus, the 2DEGs conducting thickness deserves a precise characterization in the future for accurately determining the SOT efficiency in the SrTiO$_3$-based 2DEGs systems, which is unfortunately beyond our current ability. More importantly, through controlling the Ar$^+$-etching power, time, and the chamber pressure, we may anticipate how to tune the 2DEGs conducting thickness, and probably the Rashba-Edelstein spin-splitting and SOT efficiency as well, in the Ar$^+$-etched SrTiO$_3$ 2DEGs, which may implement a more efficient spin source for SOT applications such as manipulating domain walls in racetrack memories and switching magnetic memory or logic devices.

IV. CONCLUSIONS

In summary, charge current flowing in plane in an oxide Rashba-Edelstein 2DEGs interface can generate a spin current and a strong SOT in an adjacent NiFe layer is observed by ST-FMR measurements. The calculated charge-to-spin conversion efficiency $|\theta_{CS}|$ has values up to 0.9 for Ar$^+$-etched SrTiO$_3$/NiFe, 1.8 for SrTiO$_3$/LaAlO$_3$/NiFe, and 0.6 for SrTiO$_3$/LaTiO$_3$/NiFe. These values are much larger than that of 0.07 for Pt. The spin-orbital coupling in the STO/LAO interface is probably more efficient than that of the Ar$^+$-etched STO surface. In addition, the structure of Ar$^+$-etched SrTiO$_3$/NiFe can be simply fabricated by magnetron sputtering, which is very beneficial for the SOT memory device. This research hints at alternative and promising practical applications in high energy-efficient SOT memory devices based on STO-based 2DEGs for nonvolatile memory and logic.

[1] A. Ohtomo and H. Y. Hwang, A high-mobility electron gas at the LaAlO$_3$/SrTiO$_3$ heterointerface, Nature **427,** 423 (2004).

[2] G. Herranz, M. Basletic, M. Bibes, C. Carretero, E. Tafra, E. Jacquet, K. Bouzehouane, C. Deranlot, A. Hamzic, J. M. Broto, A. Barthelemy, and A. Fert, High Mobility in LaAlO$_3$/SrTiO$_3$ Heterostructures: Origin, Dimensionality, and Perspectives, Phys. Rev. Lett. **98,** 216803 (2007).

[3] A. Brinkman, M. Huijben, M. van Zalk, J. Huijben, U. Zeitler, J. C. Maan, W. G. van der Wiel, G. Rijnders, D. H. A. Blank, and H. Hilgenkamp, Magnetic effects at the interface between non-magnetic oxides, Nat. Mater. **6,** 493 (2007).

[4] N. Reyren, S. Thiel, A. D. Caviglia, L. Fitting Kourkoutis, G. Hammerl, C. Richter, C. W. Schneider, T. Kopp, A.-S. Rüetschi, D. Jaccard, M. Gabay, D. A. Muller, J.-M. Triscone, and J. Mannhart, Superconducting interfaces between insulating oxides, Science **317,** 1196 (2007).

[5] L. Li, C. Richter, J. Mannhart, and R. C. Ashoori, Coexistence of magnetic order and two-dimensional superconductivity at LaAlO$_3$/SrTiO$_3$ interfaces, Nat. Phys. **7,** 762 (2011).

[6] N. Nakagawa, H. Y. Hwang, and D. A. Muller, Why some interfaces cannot be sharp, Nat. Mater. **5,** 204 (2006).

[7] A. Kalabukhov, R. Gunnarsson, J. Börjesson, E. Olsson, T. Claeson, and D. Winkler, Effect of oxygen vacancies in the SrTiO$_3$ substrate on the electrical properties of the LaAlO$_3$/SrTiO$_3$ interface, Phys. Rev. B **75,** 121404 (2007).

[8] P. R. Willmott, S. A. Pauli, R. Herger, C. M. Schlepütz, D. Martoccia, B. D. Patterson, B. Delley, R. Clarke, D. Kumah, C. Cionca, and Y. Yacoby, Structural Basis for the Conducting Interface between LaAlO$_3$ and SrTiO$_3$, Phys. Rev. Lett. **99,** 155502 (2007).

[9] Y. Z. Chen, et al., Extreme mobility enhancement of two-dimensional electron gases at oxide interfaces by charge-transfer-induced modulation doping, Nat. Mater. **14,** 801 (2015).

[10] A. F. Santander-Syro, O. Copie, T. Kondo, F. Fortuna, S. Pailhès, R. Weht, X. G. Qiu, F. Bertran, A. Nicolaou, A. Taleb-Ibrahimi, P. Le Fèvre, G. Herranz, M. Bibes, N. Reyren, Y. Apertet, P. Lecoeur, A. Barthélémy, and M. J. Rozenberg, Two-dimensional electron gas with universal subbands at the surface of SrTiO$_3$, Nature **469,** 189 (2011).

[11] P. D. C. King, R. H. He, T. Eknapakul, P. Buaphet, S.-K. Mo, Y. Kaneko, S. Harashima, Y. Hikita, M. S. Bahramy, C. Bell, Z. Hussain, Y. Tokura, Z. X. Shen, H. Y. Hwang, F. Baumberger, and W. Meevasana, Subband Structure of a Two-Dimensional Electron Gas Formed at the Polar Surface of the Strong Spin-Orbit Perovskite KTaO$_3$, Phys. Rev. Lett. **108,** 117602 (2012).

[12] H. R. Zhang, Y. Yun, X. J. Zhang, H. Zhang, Y. Ma, X. Yan, F. Wang, G. Li, R. Li, T. Khan, Y. S. Chen, W. Liu, F. X. Hu, B. G. Liu, B. G. Shen, W. Han, and J. R. Sun, High-Mobility Spin-Polarized Two-Dimensional Electron Gases at EuO/KTaO$_3$ Interfaces, Phys. Rev. Lett. **121,** 116803 (2018).

[13] V. M. Edelstein, Spin polarization of conduction electrons induced by electric current in two-dimensional asymmetric electron systems, Solid State Commun. **73,** 233 (1990).

[14] Q. Song, H. R. Zhang, T. Su, W. Yuan, Y. Y. Chen, W. Y. Xing, J. Shi, J. R. Sun, and W. Han, Observation of inverse Edelstein effect in Rashba-split 2DEG between SrTiO$_3$ and LaAlO$_3$ at room temperature, Sci. Adv. **3,** e1602312 (2017).

[15] E. Lesne, Y. Fu, S. Oyarzun, J. C. Rojas-Sánchez, D. C. Vaz, H. Naganuma, G. Sicoli, J.-P. Attané, M. Jamet, E. Jacquet, J.-M. George, A. Barthélémy, H. Jaffrès, A. Fert, M. Bibes, and L. Vila, Highly efficient and tunable

spin-to-charge conversion through Rashba coupling at oxide interfaces, Nat. Mater. **15,** 1261 (2016).

[16] R. Ohshima, Y. Ando, K. Matsuzaki, T. Susaki, M. Weiler, S. Klingler, H. Huebl, E. Shikoh, T. Shinjo, S. T. B. Goennenwein, and M. Shiraishi, Strong evidence for d-electron spin transport at room temperature at a LaAlO$_3$/SrTiO$_3$ interface, Nat. Mater. **16,** 609 (2017).

[17] Y. Wang, R. Ramaswamy, M. Motapothula, K. Narayanapillai, D. P. Zhu, J. W. Yu, T. Venkatesan, and H. Yang, Room-temperature giant charge-to-spin conversion at the SrTiO$_3$−LaAlO$_3$ oxide interface, Nano Lett. **17,** 7659 (2017).

[18] L. Q. Liu, C. F. Pai, Y. Li, H. W. Tseng, D. C. Ralph, and R. A. Buhrman, Spin-torque switching with the giant spin Hall effect of tantalum, Science **336,** 555 (2012).

[19] J. H. Han, A. Richardella, S. A. Siddiqui, J. Finley, N. Samarth, and L. Q. Liu, Room-Temperature Spin-Orbit Torque Switching Induced by a Topological Insulator, Phys. Rev. Lett. **119,** 077702 (2017).

[20] X. Z. Chen, R. Zarzuela, J. Zhang, C. Song, X. F. Zhou, G. Y. Shi, F. Li, H. A. Zhou, W. J. Jiang, F. Pan, and Y. Tserkovnyak, Antidamping-Torque-Induced Switching in Biaxial Antiferromagnetic Insulators, Phys. Rev. Lett. **120,** 207204 (2018).

[21] L. Q. Liu, T. Moriyama, D. C. Ralph, and R. A. Buhrman, Spin-Torque Ferromagnetic Resonance Induced by the Spin Hall Effect, Phys. Rev. Lett. **106,** 036601 (2011).

[22] See Supplemental Material at http://link.aps.org/supplemental/10.1103/PhysRevApplied.12.034004 for more detailed information about the temperature-dependent carrier concentration and mobility, ST-FMR signals at full magnetic field range, dc-biased ST-FMR experiments, ST-FMR measurements with the magnetic field applied at different angles, influence of the spin pumping effect, and the power-dependent ST-FMR results.

[23] A. R. Mellnik, J. S. Lee, A. Richardella, J. L. Grab, P. J. Mintun, M. H. Fischer, A. Vaezi, A. Manchon, E.-A. Kim, N. Samarth, and D. C. Ralph, Spin-transfer torque generated by a topological insulator, Nature **511,** 449 (2014).

[24] C. F. Pai, L. Q. Liu, Y. Li, H. W. Tseng, D. C. Ralph, and R. A. Buhrman, Spin transfer torque devices utilizing the giant spin Hall effect of tungsten, Appl. Phys. Lett. **101,** 122404 (2012).

[25] T. X. Nan, S. Emori, C. T. Boone, X. J. Wang, T. M. Oxholm, J. G. Jones, B. M. Howe, G. J. Brown, and N. X. Sun, Comparison of spin-orbit torques and spin pumping across NiFe/Pt and NiFe/Cu/Pt interfaces, Phys. Rev. B **91,** 214416 (2015).

[26] Y. Wang, P. Deorani, X. P. Qiu, J. H. Kwon, and H. Yang, Determination of intrinsic spin Hall angle in Pt, Appl. Phys. Lett. **105,** 152412 (2014).

[27] G. D. Fuchsa, J. C. Sankey, V. S. Pribiag, L. Qian, P. M. Braganca, A. G. F. Garcia, E. M. Ryan, Z. P. Li, O. Ozatay, D. C. Ralph, and R. A. Buhrman, Spin-torque ferromagnetic resonance measurements of damping in nanomagnets, Appl. Phys. Lett. **91,** 062507 (2007).

[28] O. Copie, V. Garcia, C. Bödefeld, C. Carrétéro, M. Bibes, G. Herranz, E. Jacquet, J.-L. Maurice, B. Vinter, S. Fusil, K. Bouzehouane, H. Jaffrès, and A. Barthélémy, Towards Two-Dimensional Metallic Behavior at LaAlO$_3$/SrTiO$_3$ Interfaces, Phys. Rev. Lett. **102,** 216804 (2009).

[29] K. Kondou, R. Yoshimi, A. Tsukazaki, Y. Fukuma, J. Matsuno, K. S. Takahashi, M. Kawasaki, Y. Tokura, and Y. Otani, Fermi-level-dependent charge-to-spin current conversion by Dirac surface states of topological insulators, Nat. Phys. **12,** 1027 (2016).

[30] J. Varignon, L. Vila, A. Barthélémy, and M. Bibes, A new spin for oxide interfaces, Nat. Phys. **14,** 322 (2018).

[31] W. F. Zhang, W. Han, X. Jiang, S. H. Yang, and S. S. P. Parkin, Role of transparency of platinum–ferromagnet interfaces in determining the intrinsic magnitude of the spin Hall effect, Nat. Phys. **11,** 496 (2015).

[32] Y. Liu, Z. Yuan, R. J. H. Wesselink, A. A. Starikov, and P. J. Kelly, Interface Enhancement of Gilbert Damping from First Principles, Phys. Rev. Lett. **113,** 207202 (2014).

[33] J. C. Rojas-Sánchez, N. Reyren, P. Laczkowski, W. Savero, J. P. Attané, C. Deranlot, M. Jamet, J. M. George, L. Vila, and H. Jaffrès, Spin Pumping and Inverse Spin Hall Effect in Platinum: The Essential Role of Spin-Memory Loss at Metallic Interfaces, Phys. Rev. Lett. **112,** 106602 (2014).

[34] S. S. P. Parkin, C. Kaiser, A. Panchula, P. M. Rice, B. Hughes, M. Samant, and S. H. Yang, Giant tunneling magnetoresistance at room temperature with MgO (100) tunnel barriers, Nat. Mater. **3,** 862 (2004).

[35] S. Yuasa, T. Nagahama, A. Fukushima, Y. Suzuki, and K. Ando, Giant room-temperature magnetoresistance in single-crystal Fe/MgO/Fe magnetic tunnel junctions, Nat. Mater. **3,** 868 (2004).

[36] W. X. Zhang, Q. R. Wang, B. Peng, H. Z. Zeng, W. T. Soh, C. K. Ong, and W. L. Zhang, Spin galvanic effect at the conducting SrTiO$_3$ surfaces, Appl. Phys. Lett. **109,** 262402 (2016).

[37] D. Kan, T. Terashima, R. Kanda, A. Masuno, K. Tanaka, S. C. Chu, H. Kan, A. Ishizumi, Y. Kanemitsu, Y. Shimakawa, and M. Takano, Blue-light emission at room temperature from Ar$^+$-irradiated SrTiO$_3$, Nat. Mater. **4,** 816 (2005).

[38] H. Yasuda, Y. Yamada, T. Tayagaki, and Y. Kanemitsu, Spatial distribution of carriers in SrTiO$_3$ revealed by photoluminescence dynamics measurements, Phys. Rev. B **78,** 233202 (2008).